Supplementary materials

Curvature as the Missing Descriptor of Sodium Storage in Hard Carbon

Zoya V. Bobyleva*[a], Anastasia M. Alekseeva[a], Sergey V. Ryazantsev[b], Maria A. Solovieva[a,c], Grigorii P. Lakienko[c], Yana V. Sultanova[a], Georgy S. Peters[d], Dmitry A. Aksyonov[c], Oleg A. Drozhzhin[a], Artem M. Abakumov[c], and Evgeny V. Antipov[a,c]

[a] Department of Chemistry, Lomonosov Moscow State University, 119991 Moscow, Russian Federation
[b] Faculty of Materials Science, Shenzhen MSU-BIT University, 518172 Shenzhen, China
[c] Center for Energy Science and Technology, Skolkovo Institute of Science and Technology, 121205 Moscow, Russian Federation
[d] SAXS BioMUR Beamline, National research center “Kurchatov institute”, 123182 Moscow, Russian Federation
Keywords: sodium-ion batteries, hard carbon, intercalation, mechanisms, DFT.

*Corresponding author. Department of Chemistry, Lomonosov Moscow State University, 119991, Moscow, Russian Federation
E-mail address: zoyamostovik@gmail.com (Z.V.B.)

DFT study

S.1. Construction of curved HC layers and edge passivation by hydrogen

Table S1. Results of STEM curvature radius distribution analysis before charge, at 200 mV, and 2 mV. R10, R50, and R90 represent the radii of graphene-like curved layers, where the proportion of such layers is less than 10%, 50%, and 90%, respectively.

sample	R10, Å	R50, Å	R90, Å
before charge	13.35	25.90	56.57
200 mV	13.75	23.28	39.53
2 mV	14.92	25.88	41.92

Table S2. Results of elemental analysis of HC materials obtained at different temperatures in an Ar-flow

Temperature (°C)	C (wt. %)	H (wt. %)	O (wt. %)
1300	98.73	0.11	0.42
1100	97.29	0.38	1.03
900	95.36	0.63	2.02
700	94.95	1.99	3.62
500	90.32	3.03	5.69
300	71.20	4.54	23.73

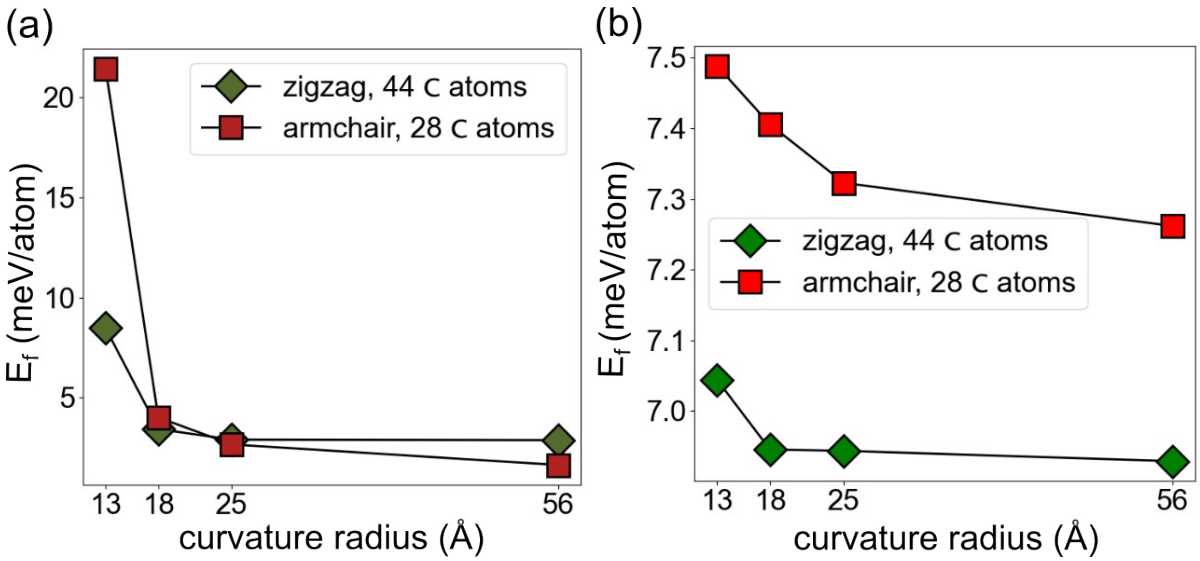

Figure S1. The formation energies of curved layers with zigzag (green line) and armchair (red line) edge structures are compared for bare (a) and H-pass (b) layers.

For hydrogen adsorption, we considered two types of passivated edges in a structure with a curvature radius of 13 Å: half-passivated (0.5 hydrogen atom per carbon atom on the edge) and fully-passivated (1 hydrogen atom per edge carbon atom). See the illustration in Fig. S2a for a visual representation. Using NIST gas thermochemical data, we estimated how the adsorption energy would change with temperature, rising from room temperature to typical annealing temperatures (300-1500 K). We assumed that in solid carbon structures, the entropic contribution was negligible and the enthalpy did not depend on temperature, with the main contribution coming from hydrogen. The adsorption energy for each temperature was calculated using Eq. S1. The resulting graph in Figure S2b shows that as the temperature increases, the adsorption energy also increases. This suggests that desorption of hydrogen from the edges may be possible and bare reconstructed edges could be present in some layers of HC domains.

$$E_{ads,\,H}(T) = \left(E_{st\_H}(0\ K) - E_{st}(0\ K) - n_H \cdot \frac{G_{H_2}(T)}{2}\right) / n_H \qquad \text{(S1)}$$

where $E_{ads,H}(T)$ stands for temperature-dependant hydrogen adsorption energy, E_{st_H} and E_{st} are the total energy of the structure with adsorbed hydrogen atom on the edge position and without it,

respectively, at 0 K, and G_{H2} is the Gibbs energy of gas hydrogen dependant on temperature. n_H represents the number of adsorbed hydrogen atoms in E_{st_H}.

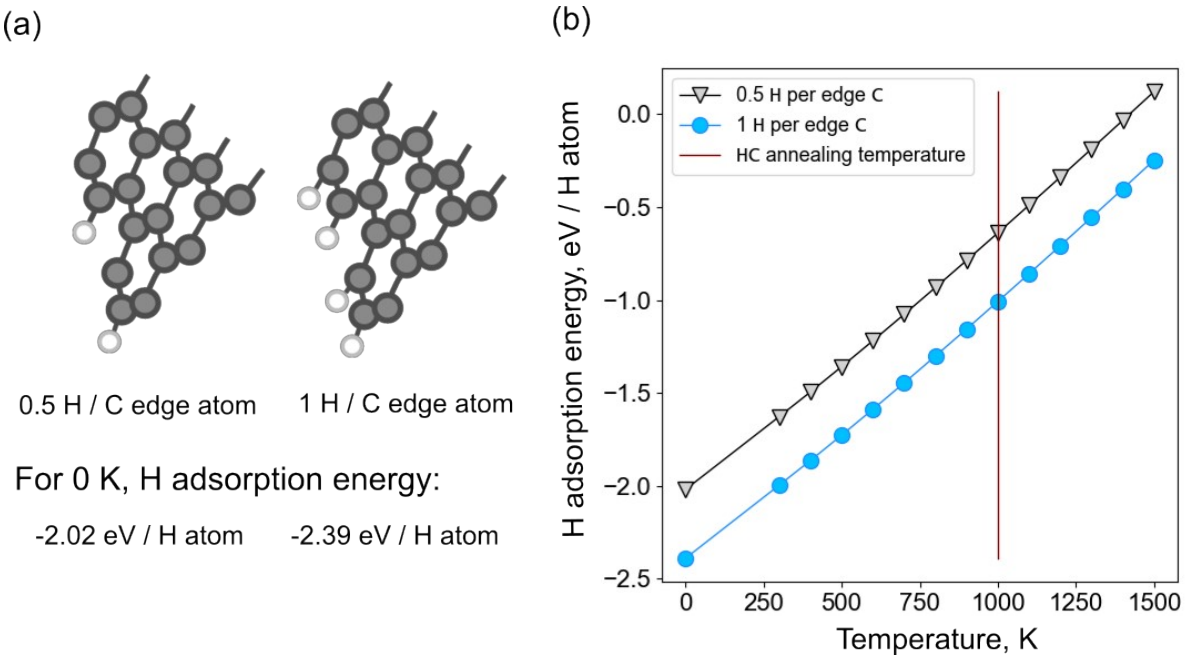

Figure S2. Mean hydrogen adsorption energy with different degrees of edge passivation, either 0.5 hydrogen atoms per edge carbon atom or 1 to 1 ratio. (a) An illustration of the edge structures and mean hydrogen adsorption energies for both cases according to DFT calculations. (b) The dependence of hydrogen adsorption energy at layer edges on temperature, with hydrogen partial pressure on the level of impurity in argon gas used in HC synthesis ($5 \cdot 10^{-7}$ bar). We have taken into account the entropy factor and the temperature dependence of the enthalpy of hydrogen gas according to Eq S1. The typical annealing temperature for HC (1000 K) is shown as the red vertical line.

Table S3. Hydrogen adsorption energy as a function of temperature (the data from Fig. S2)

Temperature, K	H adsorption energy (eV / H atom) (0.5 H atoms per edge C atom)	H adsorption energy (eV / H atom) (1 H atom per edge C atom)
0	-2.02	-2.39
300	-1.63	-2.00
400	-1.50	-1.86
500	-1.36	-1.73
600	-1.22	-1.59
700	-1.08	-1.45
800	-0.93	-1.30
900	-0.79	-1.16
1000	-0.64	-1.01
1100	-0.49	-0.86
1200	-0.34	-0.71

1300	-0.19	-0.56
1400	-0.03	-0.40
1500	0.12	-0.25

We also examined the influence of hydrogen partial pressure on hydrogen adsorption energy on the layer edges. We chose three characteristic pressures to estimate adsorption energy at a typical annealing temperature of 1000 K: the equilibrium pressure of H_2 molecule, the residual H_2 pressure in argon gas used in the annealing process, and standard pressure ($1 \cdot 10^{-7}$, $5 \cdot 10^{-7}$ and 1 bar, respectively). The results are shown in Table S3. As can be seen, the adsorption energy increases with pressure decreasing but it still stays negative at the annealing temperature of 1000 K.

Table S4. Hydrogen adsorption energy at 1000 K annealing temperature and chosen pressures for 0.5 H and 1 H per carbon edge atom.

pressure (bar)	adsorption energy (eV/H atom) (0.5 H per carbon edge atom)	adsorption energy (eV/H atom) (1 H per carbon edge atom)
$1 \cdot 10^{-7}$	-0.17	-0.69
$5 \cdot 10^{-7}$	-0.24	-0.76
$1 \cdot 10^{0}$	-0.87	-1.38

Table S5. Curved HC layer formation energy for bare and H-pass structures (from Fig. 1b).

curvature radius, Å	E_f (bare), meV/atom	E_f (H-pass), meV/atom
13	8.5	6.9
18	3.4	2.6
25	2.9	2.5
56	2.9	1.8

S.2. Impact of Stone-Wales defects on curvature

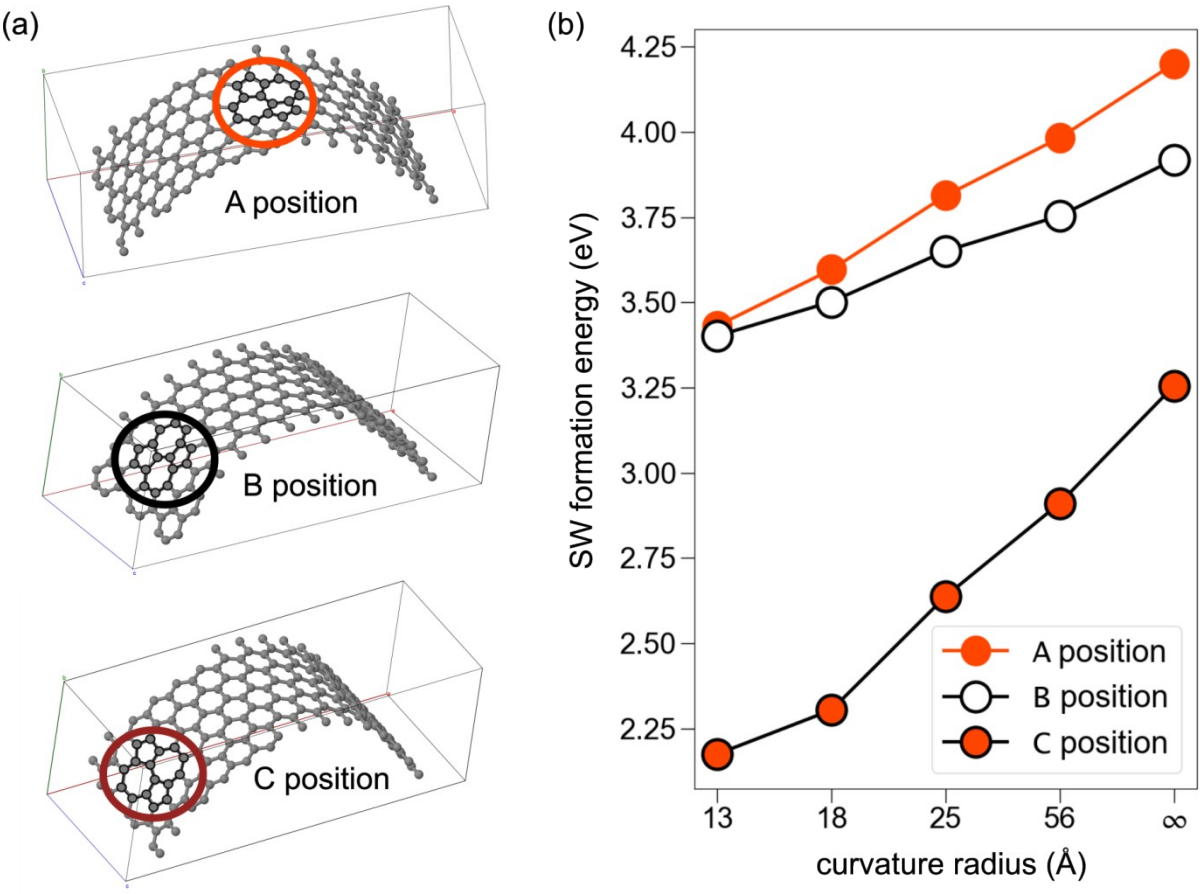

Figure S3: SW defect formation energy in different positions. The pictures of positions A, B, C (a) and SW defect formation energies in these positions for different curvature radii (b). The energy increases with increasing curvature radius for all the positions.

Firstly, we analyzed the formation energy of hydrogen-passivated structures in comparison to bare edges (Fig. 2b, orange line). The formation energy of curved carbon layers with hydrogen atoms is negligibly lower than those without hydrogen, indicating that the hydrogen has minimal impact on curvature.

The formation energy of SW defects was examined in three geometrically unequal positions A, B, and C (Fig. S3(a)) for four considered curvature radii and a graphene nanoribbon as the zero curvature of infinite radius. Several tendencies can be observed from the data shown in Fig. S3(b), representing the formation of SW defects in non-passivated curved layers.

1. In all cases, the formation energy is lower than that of a SW defect in a graphene nanoribbon or pristine graphene sheet[1]. The obtained data show that the distortion of graphene sheets with the formation of curved layers makes it easier for defects to form, which can explain the high defectiveness of HC materials and shed light on the results of Raman spectroscopy in the previous chapter of this paper. Such hypotheses were proposed in the work[2] as a conclusion for their NMR experiments. It can be concluded that in the presence of SW defects the curvature is additionally stabilized.

2. It was found that the formation energy of the SW defects decreases as the position changes from A (middle) to C (edge), especially for the edge positions. This means that for layers with non-passivated structures edge reconstruction through defect formation can be beneficial in terms of thermodynamics.

Table S6. SW defect formation energies (in eV), positions A, B, C (from Figs. 1c & S3).

Curvature radius, Å / Position of SW defect	A (center), H-pass	A (center), bare	B (quarter), bare	C (edge), bare
13	3.80	3.43	3.40	2.17
18	3.64	3.60	3.50	2.30
25	3.93	3.81	3.65	2.64
56	4.22	3.98	3.75	2.91
∞	4.31	4.20	3.92	3.26

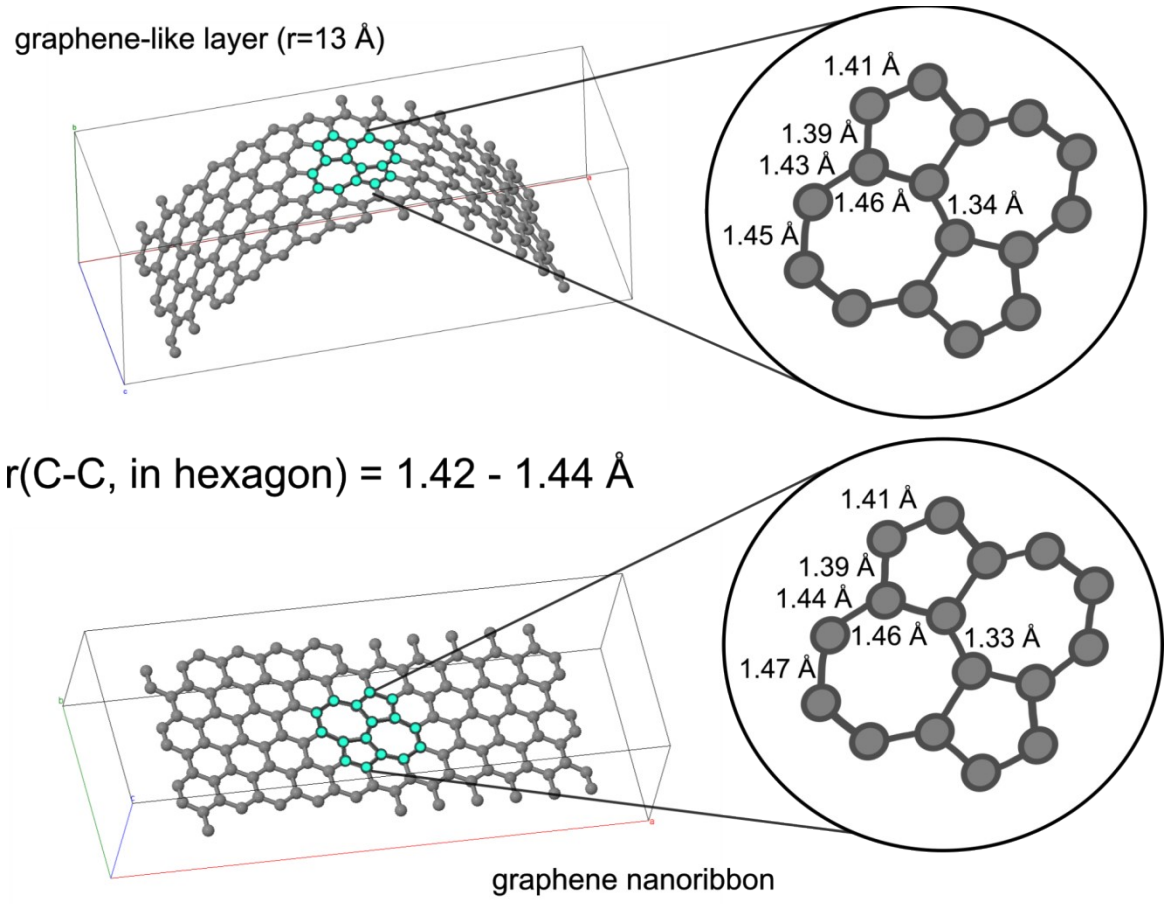

Figure S4. C-C distances in an SW defect for the two extreme cases: a graphene-like layer with a minimal curvature radius of 13 Å and a graphene nanoribbon with an infinite curvature radius. Compared to the C-C distance in hexagon fragments of the structure, the differences in the C-C distance are insignificant. For all the other layers with different curvature radii, C-C distances in SW and hexagons were within the same range of values for all the positions.

S.3. Na intercalation into Hard Carbon

Table S7. Na adsorption energies from Fig. 4.

Curvature radius, Å / Na adsorption position	no defects, bare, inside (A)	no defects, bare, outside (A)	SW defect, bare (A)	SW defect, H-pass (A)
13	0.23	0.27	-0.06	-0.06
18	0.27	0.31	-0.05	-0.09
25	0.25	0.27	-0.13	-0.11
56	0.32	0.33	-0.13	-0.11
∞	0.31	0.31	-0.23	-0.19

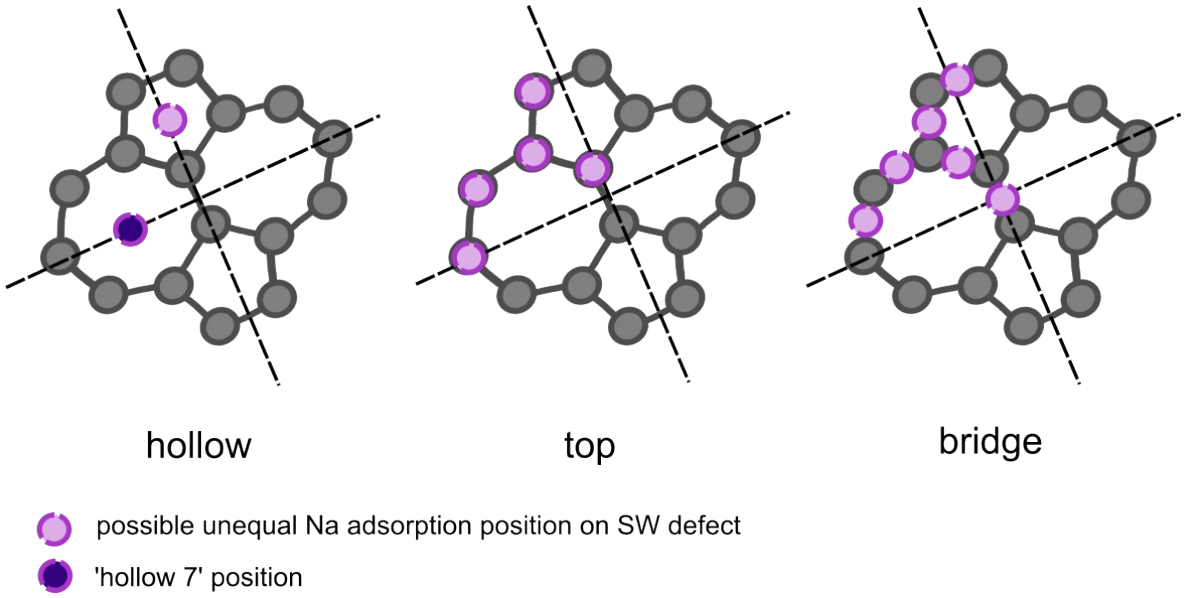

Fig. S5. Unequal positions for sodium adsorption in SW defect (hollow, top, bridge). For adsorption on SW, “hollow 7” was the only beneficial position among all others, as it appeared in all cases after optimizing atomic positions. As for the adsorption on layers without defects, the most beneficial was the “top” position.

Additionally, we investigated how Na interacts with the edges of the layers with a curvature radius of 13 Å and different structural elements in them (Fig. S4). As expected, Na does not interact with hydrogen-passivated edges. On the other hand, adsorption tends to be more beneficial on bare edges. When the edge is reconstructed with a defect (SW.C), the sodium adsorption energy increases. The structure of the considered edges is illustrated in Fig. S4.

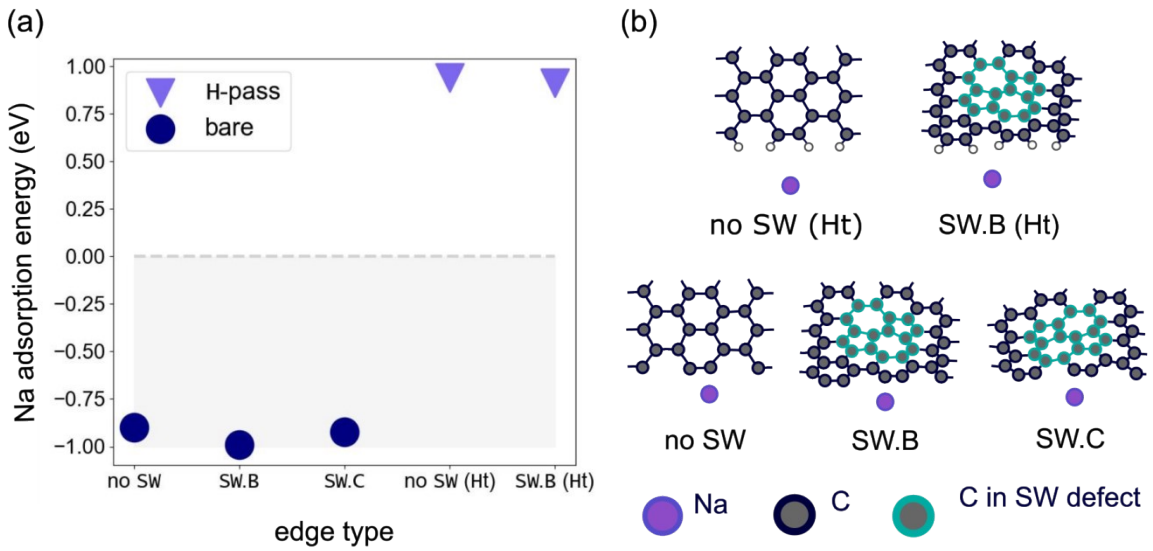

Figure S6. (a) Na adsorption energies on edges of different structures (HC with 13 A curvature radius) and (b) edge structure visualization. Minimal Na-C (for bare) and Na-H (for H-pass) distances are given in the table S5 below.

Table S8. Na adsorption energies (eV) on edges from Fig. S4 and distances between Na and C (for bare) or H (for H-pass) for edge adsorption

edge structure	no defects, bare	SW.B, bare	SW.C, bare	no defects, H-pass	SW.B, H-pass
Na adsorption energy, eV	-0.90	-0.92	-0.99	0.94	0.92
Na-X distance, Å	2.28	2.28	2.34	2.81	2.73

For all the energy calculations, we used basic parameters of VASP calculation, specifically an energy cut-off of 400 eV (ENCUT) and ISPIN=1. These parameters were chosen to balance accuracy and calculation time. We considered these parameters to be optimal, as the supercell of the HC layer with a defect contains a relatively large number of atoms (between 132 and 174, depending on the curvature radius). However, we also tested more accurate parameters (ENCUT=520 eV and ISPIN=2) to see if they were necessary for sodium adsorption energy calculations. The results of these calculations are presented in Fig. S7 and the exact values are in Table S6. A maximum difference of 0.2 eV was observed for Na adsorption on a defect-free HC layer. Edge adsorption without defects was affected by 0.1 eV. In other cases, the difference was not significant. These results allow us to conclude that adsorption can be calculated using the basic VASP parameters.

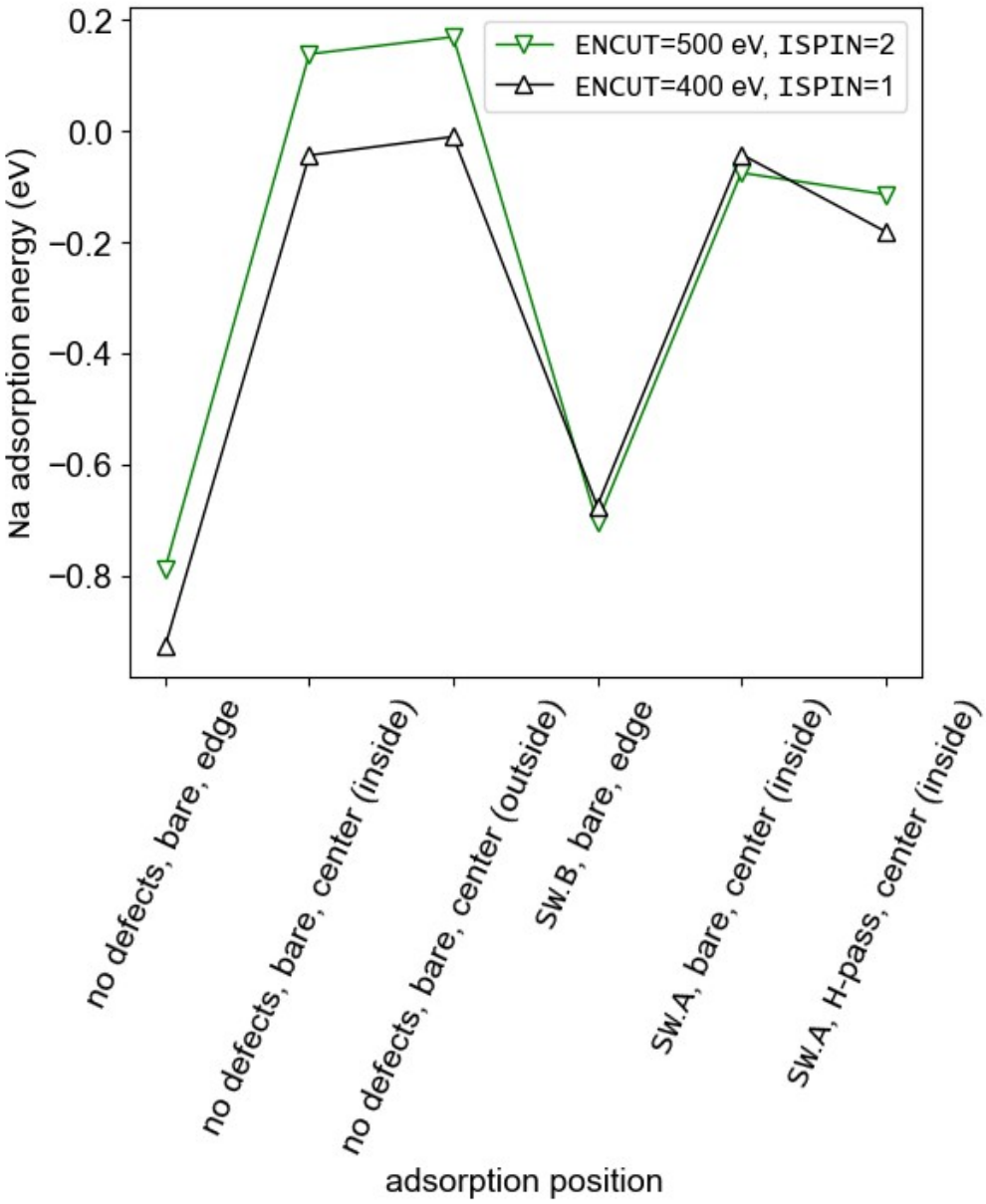

Fig. S7. Comparison of sodium adsorption energies calculated with different ENCUT and ISPIN parameters

Table S9. Comparison of sodium adsorption energies (eV) calculated with different ENCUT and ISPIN parameters (from Fig. S7)

Na adsorption position	Na adsorption energy (eV) ENCUT=400, ISPIN=1	Na adsorption energy (eV) ENCUT=520, ISPIN=2
no defects, bare, edge	-0.93	-0.79
no defects, bare, center (inside)	-0.04	0.14
no defects, bare, center (outside)	-0.01	0.17
SW.B, bare, edge	-0.67	-0.71
SW.A, bare, center (inside)	-0.04	-0.08
SW.A, H-pass, center (inside)	-0.18	-0.11

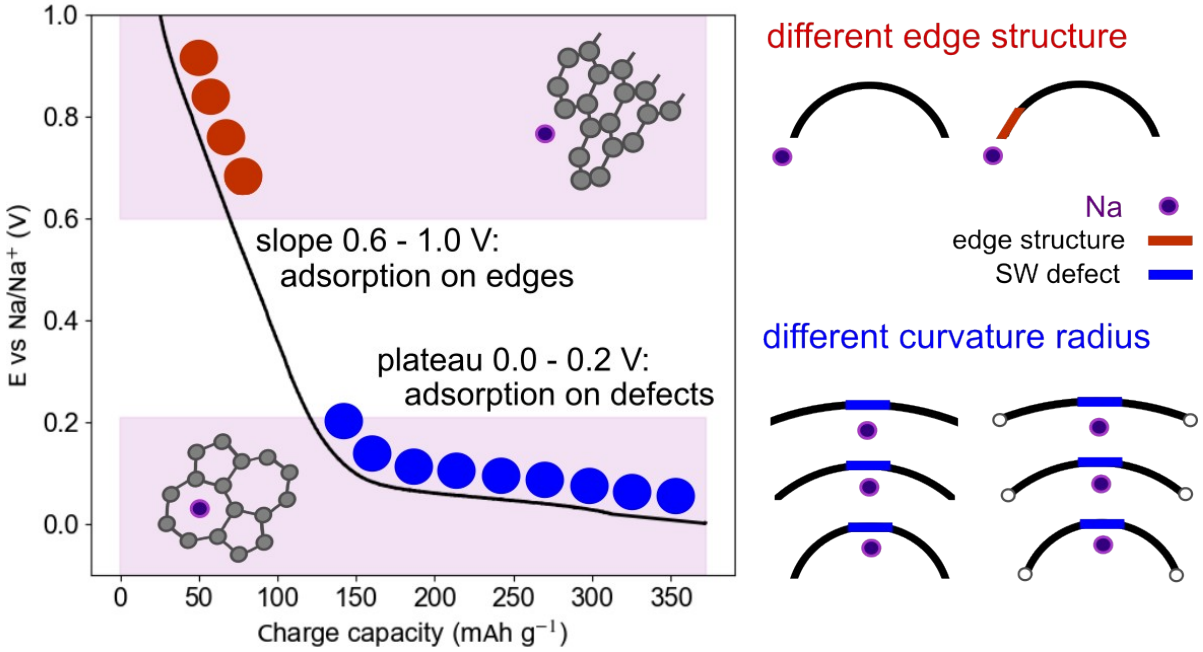

Fig. S8. The DFT calculated Na adsorption/intercalation voltages for single-layer curved graphene fragments used as a model of hard carbon. Two regions of the galvanostatic curve correspond to specific sites of sodium adsorption in the HC layer. The discharge region from 1.0 to 0.6 V vs Na/Na^+ on the sloping part of the curve is associated with edge adsorption, while the region from 0.2 to 0.0 V vs Na/Na^+ corresponds to the plateau reflecting sodium adsorption on Stone-Wales defects in layers of different curvatures and passivation states.

Herein we compare the intercalation energy of single sodium ion in models with different interlayer distance and adsorption energy in single layer notated as ∞ distance (the comparison was made for the model with initial curvature radius of 18 Å) as shown in Fig S9 and Table S10. The interlayer distances were selected to cover the range observed experimentally in various hard carbon samples.

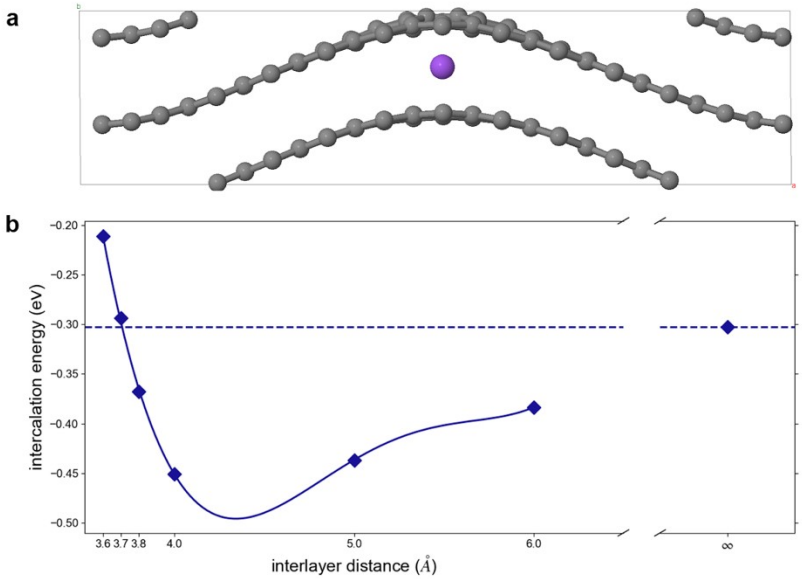

Fig. S9. (a) Layered model illustration (b) Intercalation energy of a single sodium atom on a Stone-Wales (SW) defect as a function of interlayer distance (Å) fitted with polynom. Adsorption on a single layer is denoted as infinite distance.

Table S10. Numeric values for Fig. S9.

interlayer distance (Å)	intercalation energy (eV)
3.6	-0.21
3.7	-0.29
3.8	-0.37
4.0	-0.45
5.0	-0.44
6.0	-0.38
∞	-0.30

To confirm preserving the influence of curvature in the layered model, intercalation energy between pristine layers of graphite and curved HC18 model was tested. The results are presented in Table 2. The calculations show positive influence of curvature on sodium adsorption/intercalation, the energy being lower for curved structures, и влияние более выражено.

Table S11. The comparison of adsorption / intercalation energy in flat and curved models. Adsorption energy corresponds to a single layer model and intercalation energy – to layered 3D structure.

curvature, Å	adsorption energy, eV	intercalation energy, eV

18	0.27	0.10
∞	0.31	0.48

Table S11. Reversible changes in HC recorded by various methods

Research method	The region of the galvanostatic charge curve of HC			Similar results
	Sloping 2.0 – 0.2 V vs. Na/Na^+	Inflection 0.2 – 0.05 V vs. Na/Na^+	Plateau 0.05 – 0 V vs. Na/Na^+	
PXRD *operando*	As the intensity of the $(002)_G$ peak decreases, the $(002)_G$ peak broadens			[3,4]
SWAXS *ex situ*	1. Intensity of the $(002)_G$ peak decreases 2. The position of $(002)_G$ peak shifts to the smaller angles	1. The intensity of the halo in the region of 1-5 nm^{-1} increases 2. The position of the $(002)_G$ peak shifts to the smaller angles	1. The intensity of the halo in the region of 1-5 nm^{-1} decreases significantly 2. The position of the $(002)_G$ peak shifts to the smaller angles 3. A new peak in the region of 18 – 24 nm^{-1} appears	[5–7]
Raman spectroscopy *operando*	The G band shifts from 1605 cm^{-1} to ~ 1560 cm^{-1}	The D band (1351 cm^{-1}) becomes broader	No changes	[8–10]
iDPC-STEM *ex situ*	1. Change in the interlayer distance from 3.64 ± 0.07 Å to 3.77 ± 0.06 Å 2. Decreasing of curvature radius	1. Change in the interlayer distance from 3.77 ± 0.06 Å to 3.84 ± 0.10 Å 2. Decreasing of curvature radius		This work
Linear voltammetry	Surface-controlled process	Diffusion-controlled Process	Surface-controlled process	[11]

1. M. D. Bhatt, H. Kim and G. Kim, RSC Adv., 2022, 12, 21520–21547.
2. J. Azizi, A. Groß and H. Euchner, ChemSusChem, 2024, 17, e202301493.
3. A.Beda, C. Villevieille, P. L. Taberna, P. Simon and C. Matei Ghimbeu, J. Mater. Chem. A, 2020, 8, 5558–5571.
4. D. A. Stevens and J. R. Dahn, J. Electrochem. Soc., 2001, 148, A803–A811.
5. Y. Morikawa, S. Nishimura, R. Hashimoto, M. Ohnuma and A. Yamada, Adv. Energy Mater., 2020, 10, 1903176.
6. L. Kalder, A. Olgo, J. Lührs, T. Romann, R. Härmas, J. Aruväli, P. Partovi-Azar, A. Petzold, E. Lust and E. Härk, Energy Storage Mater., 2024, 67, 103272.
7. E. M. Reynolds, J. Fitzpatrick, M. O. Jones, N. Tapia-Ruiz, H. Y. Playford, S. Hull, I. McClelland, P. J. Baker, S. A. Cussen and G. E. Pérez, J. Mater. Chem. A, 2024, 12, 18469–18475.
8. M. Anji Reddy, M. Helen, A. Groß, M. Fichtner and H. Euchner, ACS Energy Lett., 2018, 3, 2851–2857.
9. H. Euchner, B. P. Vinayan, M. A. Reddy, M. Fichtner and A. Groß, J. Mater. Chem. A, 2020, 8, 14205–14213.
10. J. S. Weaving, A. Lim, J. Millichamp, T. P. Neville, D. Ledwoch, E. Kendrick, P. F. Mcmillan, P. R. Shearing, C. A. Howard and D. J. L. Brett, ACS Appl. Energy Mater., 2020, 3, 7476–7485
11. Z. V. Bobyleva, O. A. Drozhzhin, K. A. Dosaev, A. Kamiyama, S. V. Ryazantsev, S. Komaba and E. V. Antipov, Electrochim. Acta, 2020, 354, 136647.